

RESEARCH PAPER



# A study of inhibitors of $\alpha$ -glycero- $\beta$ -D-manno-heptose-1-phosphate adenylyltransferase from *Burkholderia pseudomallei* as a potential antibiotic target

Suwon Kim, Seri Jo, Mi-Sun Kim and Dong Hae Shin

College of Pharmacy and Graduate School of Pharmaceutical Sciences, Ewha W. University, Seoul, Republic of Korea

## ABSTRACT

$\alpha$ -Glycero- $\beta$ -D-manno-heptose-1-phosphate adenylyltransferase from *Burkholderia pseudomallei* (BpHldC) is the fourth enzyme in the ADP-L-glycero- $\beta$ -D-manno-heptose biosynthesis pathway producing a lipopolysaccharide core. Therefore, BpHldC is an anti-melioidosis target. Three ChemBridge compounds purchased from ChemBridge Corporation (San Diego, CA) were found to have an effective inhibitory activity on BpHldC. Interestingly, ChemBridge 7929959 was the most effective compound due to the presence of the terminal benzyl group. The enzyme kinetic study revealed that most of them show mixed type inhibitory modes against ATP and  $\beta$ G1P. The induced-fit docking indicated that the medium affinity of ChemBridge 7929959 is originated from its benzyl group occupying the substrate-binding pocket of BpHldC. The inhibitory role of terminal aromatic groups was proven with ChemBridge 7570508. Combined with the previous study, ChemBridge 7929959 is found to work as a dual inhibitor against both HldC and HddC. Therefore, three ChemBridge compounds can be developed as a potent anti-melioidosis agent with a novel inhibitory concept.

## ARTICLE HISTORY

Received 16 December 2020  
Revised 25 February 2021  
Accepted 2 March 2021

## KEYWORDS

$\alpha$ -Glycero- $\beta$ -D-manno-heptose-1-phosphate adenylyltransferase; *Burkholderia pseudomallei*; ADP-L-glycero- $\beta$ -D-manno-heptose; ChemBridge compounds; anti-melioidosis agent

## Introduction

*Burkholderia* is a genus of Gram-negative bacteria, which has ecological, metabolic, and morphological diversity<sup>1–4</sup>. The *Burkholderia* genus belongs to the family  $\beta$ -proteobacteria, and *Burkholderia* has two major species, the Clade I and the Clade II. The most clinically important in these groups are the *B. cepacia* complex (BCC) and the *B. pseudomallei* group in the Clade I<sup>4</sup>. The BCC are pathogens that are opportunistic to immunodeficient patients and infection from those bacteria can be prevalent and fatal to cystic fibrosis patients<sup>5–7</sup>. Meanwhile, the *B. pseudomallei* group composes of four species, which are closely related (*B. pseudomallei*, *B. mallei*, *B. thailandensis*, and *B. oklahomensis*). The incidence of melioidosis has been reported in Thailand and northern Australia. In Thailand, it is in the high ranks among infectious diseases that cause the death of patients who had HIV/AIDS and tuberculosis. In northern Australia, it is the general reason for community-acquired pneumonia<sup>8</sup>.



Lipopolysaccharide (LPS) is an amphipathic glycolipid in the outer membrane of Gram-negative bacteria. Through electrostatic interactions with outer membrane proteins and divalent cations of phosphate groups on the heptoses, LPS maintains membrane stability and limits permeability of the bacterial outer membrane<sup>9–11</sup>. There are three parts composing the LPS layer: disaccharyl-lipid complex (lipid A); a core oligosaccharide; and a repeating oligosaccharide (O-antigen)<sup>12</sup>. The core oligosaccharide can be partitioned into an inner core consisting of 3-deoxy-D-manno-octulosonic acid (KDO) and heptoses, and an outer core containing hexoses and N-acetyl-D-hexosamine<sup>13</sup>.


The carbohydrate ADP-L-glycero- $\beta$ -D-manno-heptose (ADP-L- $\beta$ -D-heptose) is a substantial precursor of the inner core oligosaccharide part and is synthesised through the ADP-L- $\beta$ -D-heptose biosynthesis pathway, which includes five enzymes<sup>14</sup>.  $\alpha$ -Glycero- $\beta$ -D-manno-heptose-1-phosphate adenylyltransferase (HldC) is the fourth enzyme in the biosynthesis pathway. In many bacterial species, the enzymatic function of HldC is achieved by a bifunctional enzyme HldE composed of ATP-dependent kinase and adenylyltransferase domains. The former acts in step 2 and the latter in step 4 of the biosynthesis pathway<sup>13</sup>. However, in *B. pseudomallei*, *Neisseria meningitidis*, *N. gonorrhoeae*, etc., the two domains of the HldE protein are encoded by separate genes, *hldA* (kinase) and *hldC* (adenylyltransferase)<sup>15</sup>. Since the blockage of the HldC catalytic activity prevents the biosynthesis of heptoses of the inner core oligosaccharide of LPS, it can be a potential antibiotic target<sup>13</sup>. Thus, we screened chemical compounds for inhibitors and tried to deduce their essential structural properties to bind with inhibitors.

## Materials and methods

### Preparation of protein native BpHldC

The gene of BpHldC, *BphldC* (NCBI reference sequence: WP\_004189202.1), coding for the BpHldC protein was amplified by using primers and ligated into the amplified expression vector pB<sub>2</sub> by way of ligation-independent cloning (LIC) method. To overexpress the protein, we transformed pDNAs into *Escherichia coli* (*E. coli*) BL21 (DE3). Transformed *E. coli* cells were incubated on Luria-Bertani (LB) agar plates. Several colonies were chosen and

**CONTACT** Dong Hae Shin  [dhshin55@ewha.ac.kr](mailto:dhshin55@ewha.ac.kr)  College of Pharmacy, Ewha W. University, Seoul 03760, Republic of Korea

 Supplemental data for this article can be accessed [here](#).

© 2021 The Author(s). Published by Informa UK Limited, trading as Taylor & Francis Group.

This is an Open Access article distributed under the terms of the Creative Commons Attribution License (<http://creativecommons.org/licenses/by/4.0/>), which permits unrestricted use, distribution, and reproduction in any medium, provided the original work is properly cited.

grown in test tubes with a cap to determine the condition for culturing in bulk. In the process, a cell stock was prepared and frozen. The mass culture proceeded at 310 K with shaking. As the absorbance at 600nm of broth reached 0.6–0.8, isopropyl-β-D-1-thiogalactopyranoside was added for expression of BpHldC. The cultures of BpHldC were incubated at 298 K for 16 h in a shaking incubator. The expressed proteins contained non-cleavage N-terminal His<sub>6</sub>-tags followed by five glycines in BpHldC (MHSHHHHGGGGG). To collect cells, we centrifuged the culture fluid with a high-speed refrigerated centrifuge at 7650×g (6500 rev min<sup>-1</sup>) for 10 min at 277 K. The cultured cell pellet was suspended and fragmented using a Digital Sonifier 450 (Branson Ultrasonics Co., Danbury, CT). Cell debris was pelleted by centrifugation. Using a HisTrap column (GE Healthcare, Piscataway, NJ), affinity chromatography was done with the supernatant on an ÄKTA explorer system (GE Healthcare, Piscataway, NJ). Ion-exchange chromatography has been done as the secondary purifications using a 5 ml Hi-Trap Q column (GE Healthcare, Piscataway, NJ).

The purified native proteins were concentrated to adequate concentration for use in the assay.

**Preparation of protein native HddC and KdsB**

HddC proteins from *B. pseudomallei*, *Campylobacter jejuni*, *E. coli*, and *Prevotella sp. 10(H)* have been purified according to the previous method<sup>16</sup>. In brief, affinity chromatography was done and ion-exchange chromatography has followed as the secondary purifications. KdsB proteins from *B. pseudomallei*, *C. jejuni*, *Chlamydia psittaci*, *E. coli*, *Klebsiella aerogenes*, *N. meningitidis*, *Pseudomonas aeruginosa*, *Salmonella enterica*, and *Vibrio cholerae* have been purified according to the previous method<sup>17</sup>. Purification was also carried out with the same process. Glucose-1-phosphate thymidyltransferase from *P. aeruginosa* has been also purified with a similar protocol as above sugar nucleotidyltransferases (SNTs).

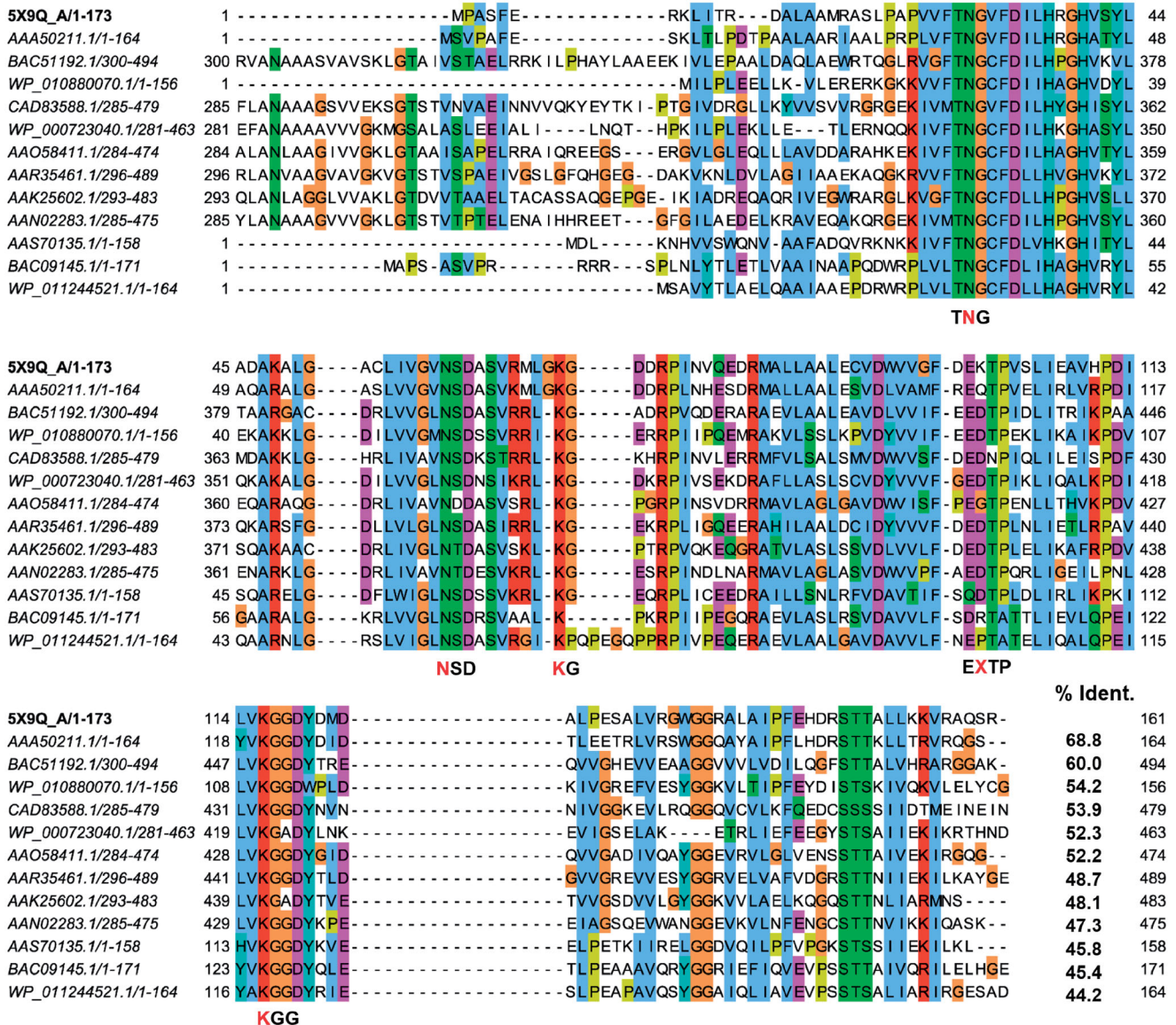


**Figure 1.** A multiple sequence alignment among BpHldC and its homologs. The predicted D-glycero-β-D-manno-heptose-1-phosphate (βH1P) binding sites were based on the docking experiment obtained after selecting 12 BpHldC homologs. The predicted substrate-binding motifs, TNG, NSD, KG, EXTP, and KGG, are indicated and the red characters represent the residues that took part in the interaction with βH1P. In the case of the EXTP motif, X represents any amino acids. In the docking result, the X residue is Lys100. Interestingly, the backbone oxygen was involved in the interaction with βH1P.



### Chemical screening with a malachite green assay method

The screening of about 150 chemical compounds (Table S1) was performed with a malachite green assay method<sup>18</sup>. The principle of this method is: when SNTs transfer the AMP moiety from ATP to the heptose, ADP-*D*-glycero- $\beta$ -*D*-manno-heptose and pyrophosphate (PPi) are produced. PPi was decayed into two phosphates by inorganic pyrophosphatase (IPP) and phosphates were measured by the malachite green method.  $\beta$ -*D*-Glucose-1-phosphate ( $\beta$ G1P) was purchased from Tokyo Chemical Industry Co. (Tokyo, Japan); TCI was used as a substrate because it is difficult to obtain the actual substrate, *D*-glycero- $\beta$ -*D*-manno-heptose-1-phosphate ( $\beta$ H1P). The content of the  $\alpha$ -form of this product was less than 0.1% in the current lot. A colour reagent of the malachite green method for phosphate detection was a mixture of ammonium molybdate ((NH<sub>4</sub>)<sub>6</sub>Mo<sub>7</sub>O<sub>24</sub>), malachite green solution and Tween 20 in the ratio 1:3:0.1. The mixture was filtered with a PVDF syringe filter and stood at room temperature (RT) for 1 h before use. All chemicals (25  $\mu$ M) were tested for their inhibitory potential through a comparison of actual absorbances with control at 620 nm. The actual absorbance was obtained from the difference in absorbance between the reaction mixtures with and without *Bp*HldC. The reaction mixture included 10 mM Tris-HCl (pH 7.5), 10 mM MgCl<sub>2</sub>, 0.04 unit IPP, and 0.025 mg ml<sup>-1</sup> *Bp*HldC (1.3  $\mu$ M). To evaluate the accuracy of the inhibitor screening, *Z'* factor was determined to be 0.9 (*n* = 15). The results indicate that the accuracy of the enzyme inhibitor test using this method is excellent<sup>19</sup>.

### Enzyme kinetics of *Bp*HldC

The malachite green assay method<sup>18</sup> was used to study the steady-state kinetics of *Bp*HldC. For the kinetic studies, reaction mixtures including 5 mM Tris-HCl (pH 7.5), 10 mM MgCl<sub>2</sub>, 0.04 unit IPP, and 0.025 mg ml<sup>-1</sup> *Bp*HldC with different concentrations of ATP (0.0039–1.5 mM) at the constant concentration of  $\beta$ G1P (1 mM) and with different concentrations of  $\beta$ G1P (0.0039–2.5 mM) at the constant concentration of ATP (0.5 mM) were used. After incubation at RT for an hour, 40  $\mu$ l of reaction mixtures were mixed with the malachite reagent (160  $\mu$ l). The mixtures were left for standing for 10 min to develop the colour. The standard curve fitting was performed using GraphPad Prism version 8.3.0 for Windows (GraphPad Software, San Diego, CA, [www.graphpad.com](http://www.graphpad.com))<sup>20</sup>.

### The IC<sub>50</sub> values of ChemBridge compounds

The malachite green assay method was also used to study the dose-dependent inhibitory effect of ethyl 5-([5-benzyl-1,3,4-oxadiazol-2-yl]thio)acetyl)amino)-4-cyano-3-methyl-2-thiophenecarboxylate (ChemBridge 7929959), ethyl 5-([5-(4-chlorophenyl)-1,3,4-oxadiazol-2-yl]thio)acetyl)amino)-4-cyano-3-methyl-2-thiophenecarboxylate (ChemBridge 7933420), and ethyl 4-cyano-5-([5-(2-ethoxyphenyl)-1,3,4-oxadiazol-2-yl]thio)acetyl)amino]-3-methyl-2-thiophenecarboxylate (ChemBridge 7991890) purchased

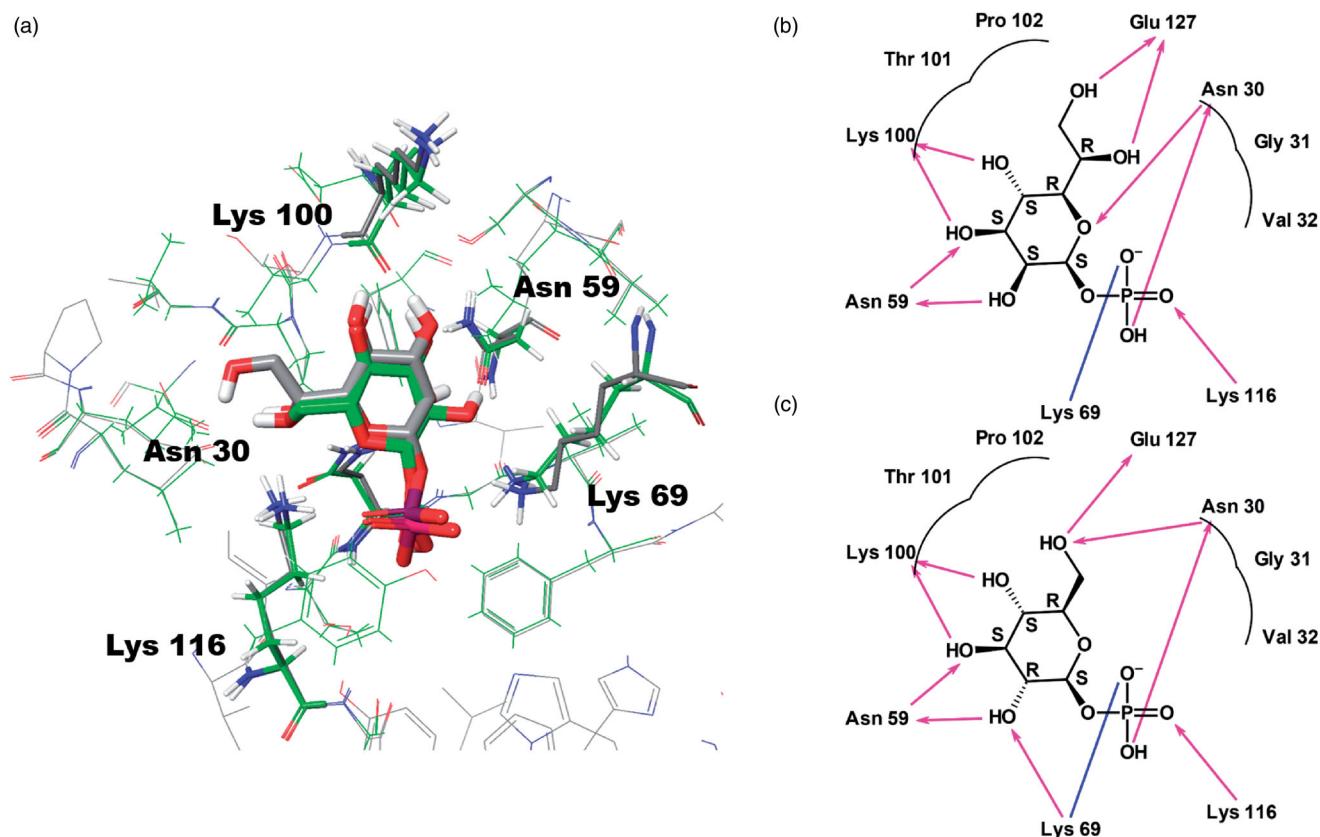


**Figure 2.** Predicted docking modes of *D*-glycero- $\beta$ -*D*-manno-heptose-1-phosphate ( $\beta$ H1P) and  $\beta$ G1P in the catalytic site of *Bp*HldC. The presumed substrate binding sites were obtained based on the X-ray crystal structure of three homologues complexed with their substrates (PDB ID: 1H1T, 1N1D, 3HL4). (a) The superimposed view of  $\beta$ H1P and  $\beta$ G1P docked on the active site (grey,  $\beta$ H1P; green,  $\beta$ G1P). The substrates and functionally important residues Asn 30, Asn 59, Lys 69, Lys 100, and Lys 116 were depicted with a stick model. All residues belong to putative substrate-binding motifs (Figure 1). In the case of Lys 100, the backbone oxygen participates in the interaction. In addition, 2D schematic representations of the docked (b)  $\beta$ H1P and (c)  $\beta$ G1P with *Bp*HldC were drawn. Figures were created with Maestro v11.5.011 and ChemDoodle v10.1.0 (iChemLabs™). The blue line represents ion interactions and the pink arrows represent the hydrogen bonds. According to the induced-fit docking results, the glide *g*-scores of substrates in the binding site pocket were -6.68 for  $\beta$ H1P and -6.59 for  $\beta$ G1P.

from ChemBridge Corporation (San Diego, CA). The 40  $\mu\text{l}$  of reaction mixtures containing 5 mM Tris-HCl (pH 7.5), 10 mM  $\text{MgCl}_2$ , and 0.05  $\text{mg ml}^{-1}$  *BpHldC* with different concentrations of ChemBridge 7929959 (0.0245–100  $\mu\text{M}$ ), 7991890 (0.0245–250  $\mu\text{M}$ ), 7933420 (0.0245–250  $\mu\text{M}$ ) were incubated at RT for an hour. The reaction mixtures lacking *BpHldC* with the same concentration of ChemBridge compounds (7929959, 7933420, and 7991890) used as above were also incubated at RT for an hour and measured as blanks. The reaction was initiated by adding 1 mM  $\beta\text{G1P}$  and 0.5 mM ATP and stood for an hour. After incubation, 160  $\mu\text{l}$  of the same malachite reagent used above was added and left for standing for 10 min. The absorbance was measured at 620 nm using the microplate spectrophotometer (Spectramax 190, Molecular Devices Corporation, Sunnyvale, CA). The percentage reactivity (% Reactivity) was calculated depending on the difference in absorbance of whether *BpHldC* was present or not in the reaction mixtures with ChemBridge compounds. The  $\text{IC}_{50}$  values of the ChemBridge compounds of *BpHldC* were calculated and plotted by a nonlinear regression analysis using GraphPad Prism 8.3.0 (GraphPad Software, San Diego, CA).

### Inhibitory enzyme kinetics

ATP concentrations were varied at the range of 0.0078–1.5 mM and 1 mM  $\beta\text{G1P}$ , the saturated concentration, was mixed with the reaction mixture with 10 mM Tris buffer (pH 7.5) at RT in a 96-well microplate. On the other hand, when  $\beta\text{G1P}$  concentrations were varied at 0.0078–2.5 mM, the ATP concentration was constant at 0.5 mM. Components of the reaction mixture were the same as those of enzyme kinetic assay but compounds were also added with 0  $\mu\text{M}$  (DMSO), 2.5  $\mu\text{M}$ , 5  $\mu\text{M}$ , 10  $\mu\text{M}$ , 20  $\mu\text{M}$ , and 40  $\mu\text{M}$ , respectively. The data obtained from the spectrophotometer were used for fitting steady-state kinetic graphs and secondary plots using the GraphPad Prism program (GraphPad Software, San Diego, CA).

### Ligand preparation, target preparation, and induced-fit docking

All the docking and scoring calculations were executed using the Schrödinger software suite (Maestro, version 11.8.012). The ChemBridge compounds were extracted from the Hit2Lead homepage, ChemBridge Chemical Store, in SDF format and were combined in one file. The SDF files of  $\beta\text{H1P}$  and  $\beta\text{G1P}$ , substrates of *BpHldC*, were got from the PubChem database. The files were

imported into Maestro and prepared for docking using Ligand Preparation. The atomic coordinates of the crystal structure of *BpHldC* (PDB ID: 5X9Q) were obtained from the Protein Data Bank and prepared by removing all solvent and adding hydrogens and minimal minimisation using Protein Preparation Wizard. Ioniser was used to generate an ionised state of all compounds at the target pH  $7.0 \pm 2.0$ . The input for an induced-fit docking is the prepared low-energy ligand forms. The induced-fit docking protocol<sup>20</sup> was worked on the graphical user interface, Maestro 11.8.012 linked with the Schrödinger software. Receptor sampling and refinement were conducted for residues within 5.0 Å of each ligand and for each ligand-protein complex. With Prime<sup>21</sup>, a side-chain sampling and prediction module, as well as the backbone of the target protein, were energy minimised. A total of induced-fit receptor conformations was generated for three ChemBridge compounds and two substrates. Finally, the ligand poses were scored using a combination of Prime and Glide Score scoring functions<sup>22</sup>.

## Results

### Chemical screening with a malachite green assay method

The enzyme kinetic study of *BpHldC* was performed and the chemical screening of about 150 compounds was done with the malachite green assay method. In this assay, the amount of inorganic phosphate was measured after pyrophosphatase treatment. It is a fast, reproducible, colorimetric method for measuring inorganic free phosphate in aqueous solutions. Hence, the assay offered great ease of exploring potent inhibitors against *BpHldC*. A list of compounds is provided in Table S1 of the Supporting Information. In order to perform the assay, a natural substrate was required. Unfortunately, the natural substrate of *HldC*,  $\beta\text{H1P}$ , was not commercially available. Even worse, the closest derivative of the natural substrate,  $\beta\text{-D-mannose-1-phosphate}$  ( $\beta\text{M1P}$ ), also was not commercially available. Nevertheless, the problem could be overcome by using  $\beta\text{G1P}$  as an alternative substrate. The feasibility of  $\beta\text{G1P}$  as a surrogate of  $\beta\text{H1P}$  was tested with an *in silico* docking experiment. The putative substrate-binding pocket was predicted using approximately 5000 homologue sequences of *BpHldC* with more than  $\sim 44\%$  sequence identity (Figure 1). Three substrate-complexed structures (PDB ID: 1N1D, 1H1T, 3HL4) of *BpHldC* homologues were also considered since their high overall topological similarity as shown in DALI z-scores; 16.0, 10.7, and 12.9, respectively. Two compounds display similar binding modes at the catalytic pocket as shown in Figure 2. Luckily,  $\beta\text{G1P}$  worked

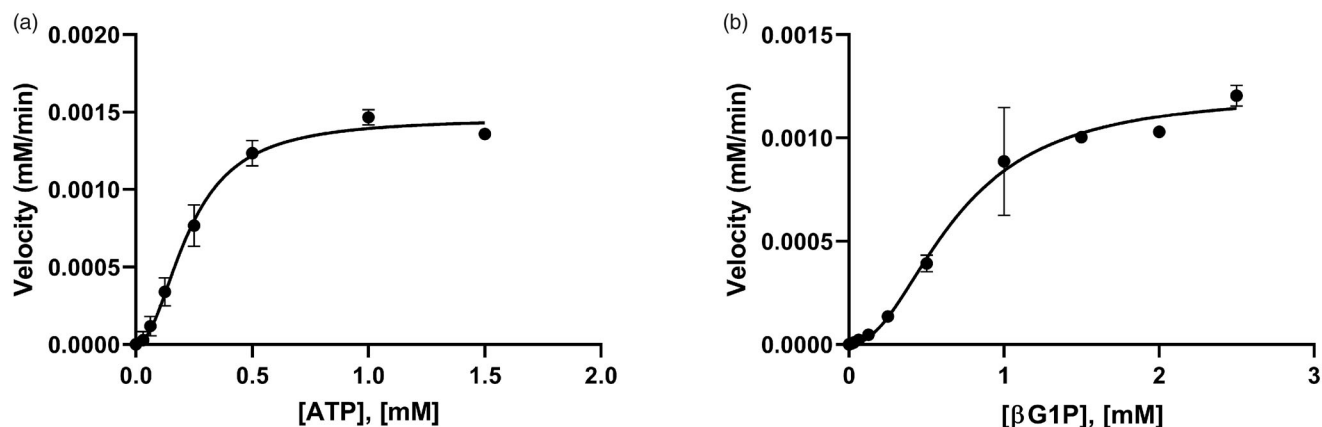


**Figure 3.** The allosteric activities of *BpHldC*. The enzyme activities with (a) various concentrations of ATP with 1 mM  $\beta\text{G1P}$  and (b) various concentrations of  $\beta\text{G1P}$  in the presence of 0.5 mM ATP. The graphs indicated that the maximum velocities were obtained at 0.5 mM ATP in the presence of 1 mM  $\beta\text{G1P}$  and 1 mM  $\beta\text{G1P}$  in the presence of 0.5 mM ATP, respectively. Each dot is expressed as the mean  $\pm$  standard error of the mean ( $n=3$ ).

as an alternative to  $\beta$ H1P for HldC. Therefore,  $\beta$ G1P was provided as a substrate to assay HldC. A similar approach was reported for searching inhibitory compounds of *D-glycero- $\alpha$ -D-manno-heptose-1-phosphate* guanylyltransferase from *Yersinia pseudotuberculosis* (YpHddC)<sup>16</sup>.  $\alpha$ -D-Mannose-1-phosphate ( $\alpha$ M1P) behaved effectively as a surrogate substrate instead of the natural substrate of YpHddC, *D-glycero- $\alpha$ -D-manno-heptose-1-phosphate*. After a round of screening, three ChemBridge compounds (7929959, 7933420, and 7991890) blocking the catalytic activity of BpHldC were detected as potential inhibitors.

### Enzyme kinetics of BpHldC

To determine the kinetic parameters of BpHldC for  $\beta$ G1P and ATP, enzyme assays were performed with various concentrations of ATP at a constant  $\beta$ G1P concentration (1 mM) and with various concentrations of  $\beta$ G1P at a constant ATP concentration (0.5 mM). The graphs of the velocities vs. concentrations of  $\beta$ G1P and ATP are shown in Figure 3. Both substrates vs. velocity plots of BpHldC were well matched with an allosteric sigmoidal model. The kinetic parameter values of BpHldC with respect to ATP at the steady-state under the constant concentration of  $\beta$ G1P (1 mM) were  $0.23 \pm 0.02$  mM for  $K_{\text{half}}$  (equals to  $EC_{50}$ ) and  $0.05 \pm 0.02$  mM for  $K_{\text{prime}}$  (related to the  $K_m$ ). Those of BpHldC with respect to  $\beta$ G1P under the constant concentration of ATP (0.5 mM) were  $0.68 \pm 0.07$  mM for  $K_{\text{half}}$  and  $0.45 \pm 0.14$  mM for  $K_{\text{prime}}$ . All parameters were calculated using the GraphPad Prism software (San Diego, CA).

### The $IC_{50}$ values of ChemBridge compounds

The inhibitory effect of three ChemBridge compounds against BpHldC was found through the chemical screening with the malachite green assay method. Therefore, the dose-dependent inhibitory effect of the ChemBridge compounds was pursued and estimated at the saturated substrate concentrations (0.5 mM ATP and 1 mM  $\beta$ G1P). The results were plotted as log inhibitor concentration vs. percentage reactivity calculated from absorbance (Figure 4).  $IC_{50}$  values determined from the dose-dependent inhibitory curves of ChemBridge compounds against BpHldC: ChemBridge 7929959 was 10.92  $\mu$ M; ChemBridge 7933420 was 17.46  $\mu$ M; ChemBridge 7991890 was 47.11  $\mu$ M.

### Inhibitory enzyme kinetics

The inhibitory kinetic assay was carried out with varying concentrations of one substrate (ATP) at the fixed concentration of the other substrate ( $\beta$ G1P) in different concentrations or vice versa regarding three ChemBridge compounds. Raw data were obtained using the spectrophotometer. Steady-state inhibitory enzyme kinetics plots were fitted by the allosteric sigmoidal model (Figure 5).

The secondary plots were used to determine the inhibitory profile of BpHldC<sup>23</sup>. Alpha values (the ratio of  $K'_i/K_i$ ) classifying inhibitory modes of inhibitor compounds were obtained with inhibition constants ( $K'_i$  and  $K_i$ ) determined from  $1/V_{\text{max}}$  vs.  $[I]$  for  $K'_i$  and slope ( $K_m/V_{\text{max}} \approx K_{\text{prime}}/V_{\text{max}}$ ) vs.  $[I]$  for  $K_i$  based on the graphs from Figure 5. Inhibitors with an approximate alpha value of 1.0 belong to a non-competitive type. The values which get to zero and which get to infinite statistically correspond to uncompetitive and competitive types, respectively. The mixed type model is determined when the alpha value exceeds 1.0. The results for ChemBridge compounds on BpHldC are shown in Table

1. The inhibition type of ChemBridge compounds appeared in the mixed-type or uncompetitive type inhibition mechanisms for ATP and the mixed-type inhibition for  $\beta$ G1P.

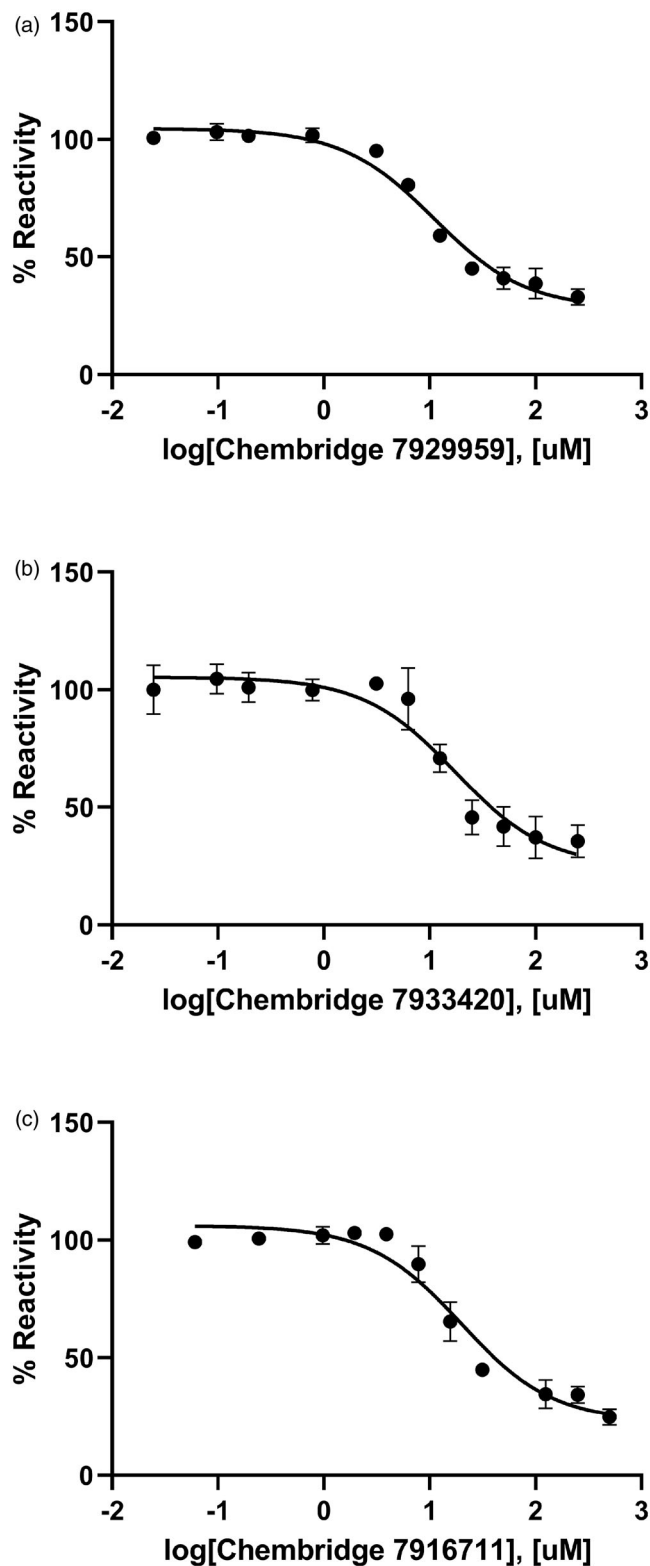


**Figure 4.** Dose-dependent inhibitory curves for the inhibition of BpHldC by ChemBridge (a) 7929959, (b) 7933420, and (c) 7991890. Each data point represents the effect of each inhibitory compound against BpHldC compared to the control. The %Reactivities are plotted against the log-concentration of inhibitory compounds. Each dot is expressed as the mean  $\pm$  standard error of the mean ( $n=3$ ).

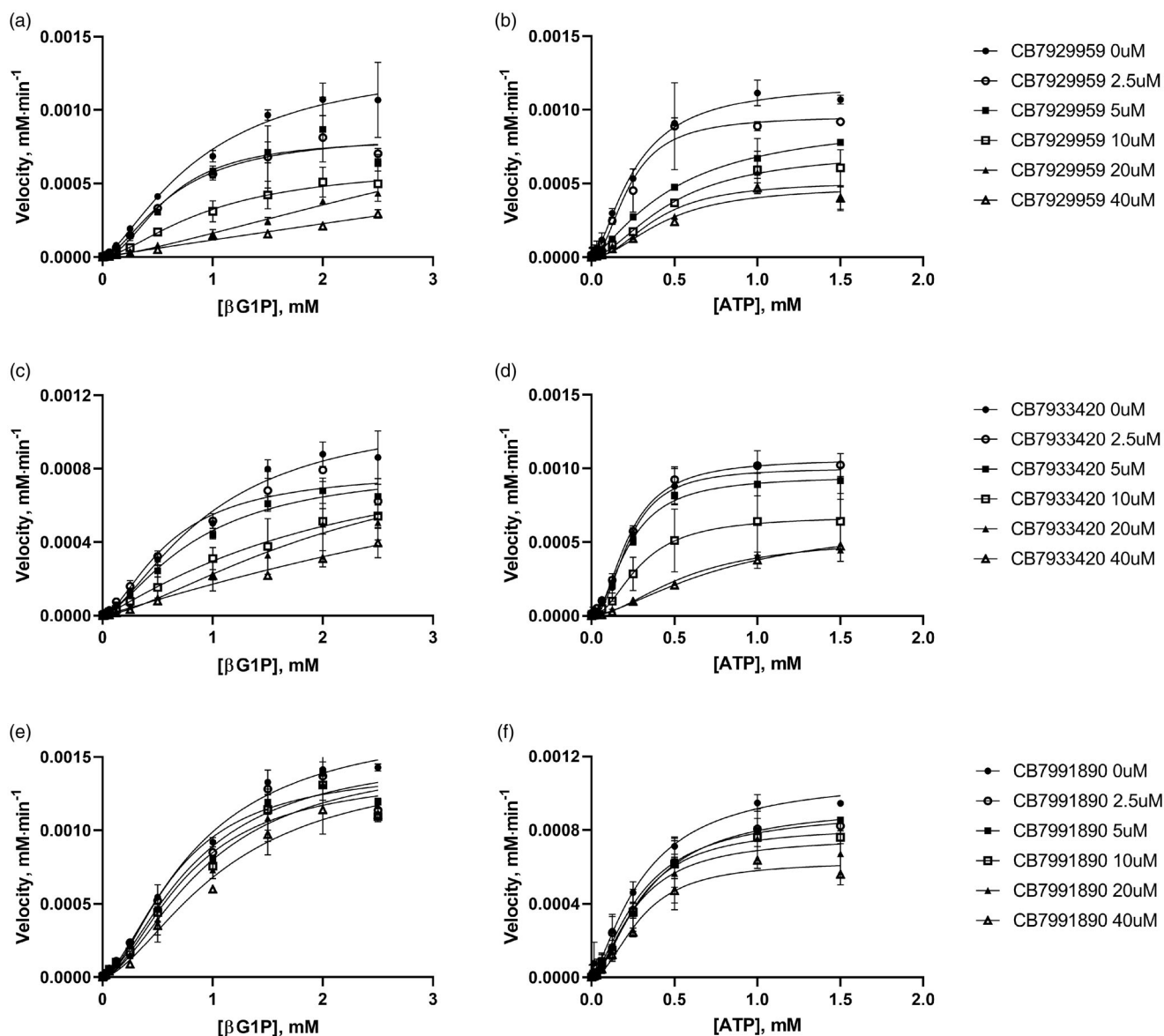


**Figure 5.** Inhibitory enzyme kinetics of *BpHldC* with ChemBridge 7929959 (CB7929959) (a, b), ChemBridge 7933420 (CB7933420) (c, d), and ChemBridge 7991890 (CB7991890) (e, f). (a, c, e) Steady-state kinetics with inhibitors regarding ATP at a fixed concentration of 1 mM  $\beta$ G1P. (b, d, f) Inhibition of *BpHldC* by compounds at varying  $\beta$ G1P concentrations with a constant concentration of 0.5 mM ATP is presented. Compounds were treated to each point with six concentrations (0, 2.5, 5, 10, 20, and 40  $\mu$ M). Each dot is expressed as the mean  $\pm$  standard error of the mean ( $n=3$ ).

**Table 1.** Inhibitory properties of compounds with *BpHldC*<sup>a</sup>.

Compounds	ATP			$\beta$ G1P		
	$K_i'$ ( $\mu$ M)	$K_i$ ( $\mu$ M)	Type	$K_i'$ ( $\mu$ M)	$K_i$ ( $\mu$ M)	Type
ChemBridge 7929959	15.59	0.43	Mixed type <sup>b</sup>	11.08	0.15	Mixed type
ChemBridge 7933420	18.46	6.80	Mixed type	568.8	6.02	Mixed type
ChemBridge 7991890	56.46	Infinite <sup>c</sup>	U.C. <sup>d</sup>	50.81	39.55	Mixed type

<sup>a</sup>All parameters were calculated using GraphPad Prism program (GraphPad Software, San Diego, CA).

<sup>b</sup>The mixed type includes properties of both competitive and non-competitive inhibition<sup>23</sup>.

<sup>c</sup>The graph was close to parallel to the X-axis.

<sup>d</sup>U.C.: un-competitive type.

### Ligand preparation, target preparation, and induced-fit docking

To deduce the binding modes of ChemBridge compounds with *BpHldC* at a molecular level, an in-depth theoretical investigation with an induced-fit docking study using the Schrödinger program was carried out (Figure 6(a,b)). The crystal structure of *BpHldC*

deposited in the Protein Data Bank (PDB ID: 5X9Q) was retrieved and docked with ChemBridge compounds to predict their binding modes. In the asymmetric unit of the crystal structure of *BpHldC*, there are four chains and two of them were determined with 4-morpholineethanesulfonic acid (MES) of which the sulphonic acid moiety bound with Lys69 at the centre of the active site composed of sugar and nucleotide-binding pockets. We used the chain D for docking because it contains MES and mimics a substrate-bound closed conformation. The docking pocket was defined based on the structural comparison of *BpHldC* with its homologues complexed with their substrates (PDB ID: 1N1D, 1H1T, 3HL4). As a result, putative substrate and nucleotide-binding cavities of *BpHldC* were searched. Top-ranked structures with the highest glide  $g$ -scores from the induced-fit docking results were surveyed. According to the induced-fit docking results, the glide  $g$ -scores of structures that were reasonably docked in the active site pocket were  $-8.30$  for ChemBridge 7929959,  $-7.38$  for ChemBridge 7933420, and  $-5.23$  for ChemBridge 7991890. The



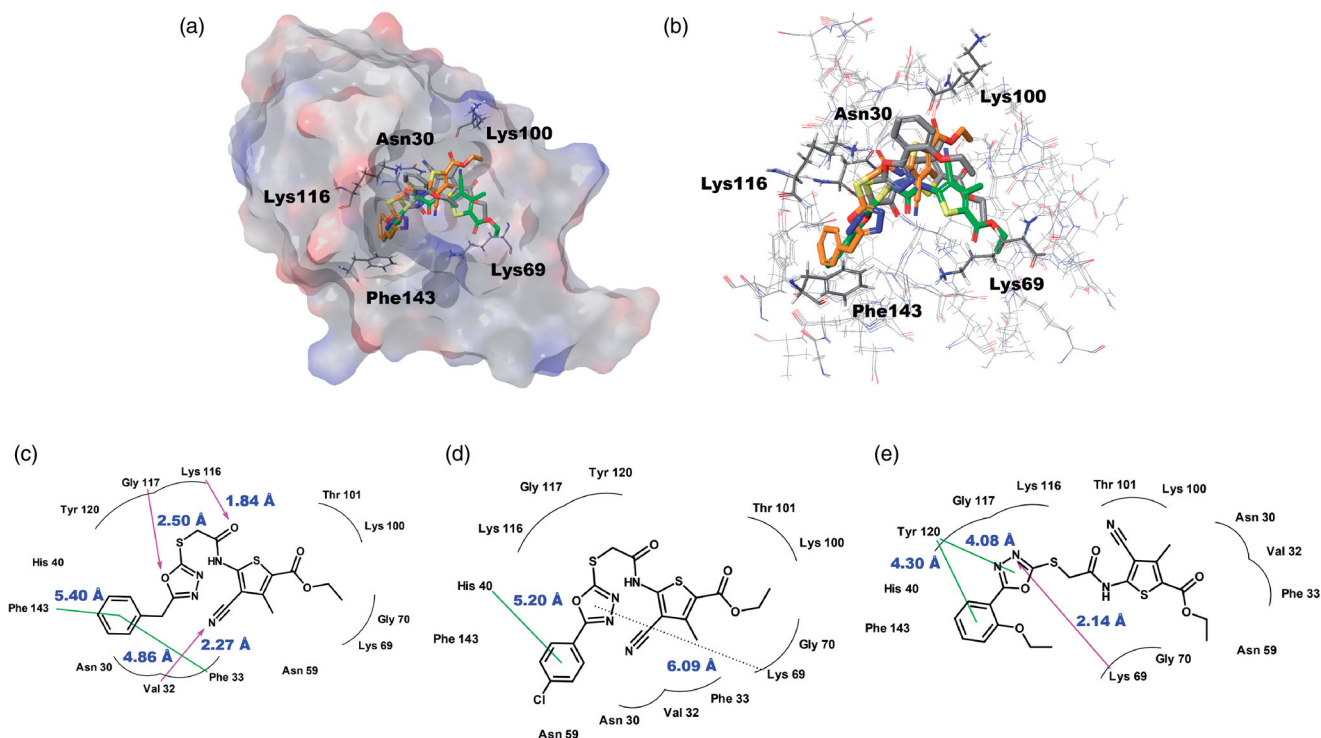


**Figure 6.** Predicted docking modes of ChemBridge compounds in the catalytic site of *BpHldC*. (a) The docking pose of ChemBridge 7929959 (orange), 7933420 (green), and 7991890 (grey) were depicted on the electrostatic surface potential of *BpHldC* (red, negative; blue, positive; white, uncharged). (b) The superimposed view of ChemBridge compounds docked on the active site. Functionally important residues Asn 30, Lys69, Lys100, Lys116, and Phe143 were depicted with a stick model according the docking mode of ChemBridge 7929959. In addition, 2D schematic representations of the docked ChemBridge compounds with *BpHldC* were drawn. (c) ChemBridge 7929959, (d) ChemBridge 7933420, and (e) ChemBridge 7991890. Figures were created with Maestro v11.5.011 and ChemDoodle v10.1.0 (iChemLabs<sup>TM</sup>). The pink arrows represent the hydrogen bonds. The green line represents the  $\pi$ - $\pi$  interaction and the dotted line represents the  $\pi$ -cation interaction. Comparison with other substrate-bound crystal structures of *BpHldC* homologues revealed that Phe143 former locates in the nucleotide binding cavity and Lys69 interacts with the phosphate moiety of nucleotide. The residues in the highly conserved substrate binding motifs (Figure 1) are drawn with curved lines.

predicted complex structures and 2D schematic representations are illustrated in Figure 6(c–e). The docking study with the three ChemBridge compounds indicated that the order of the glide  $g$ -scores was well-matched with their experimental inhibitory capability ( $IC_{50}$ ).

## Discussion

The ADP-L- $\beta$ -D-heptose biosynthesis pathway is one of three major pathways including GDP-6-deoxy- $\alpha$ -D-manno-heptose and CMP-3-deoxy-D-manno-octulosonic acid biosynthesis pathways, which produces carbohydrates in the core oligosaccharide part of LPS. We assayed inhibitory activities of compounds with an in-house chemical library (Table S1) based on the expanded version of the previous one<sup>16</sup> against the adenylyltransferase activity of HldC from *B. pseudomallei* (*BpHldC*). We found that compounds having a similar scaffold showed inhibitory activities against *BpHldC*. Hence, we attempted to bring out the structural meaning and move towards the development of inhibitors that have a better affinity.

In brief, the docking modes of three chemicals can explain their inhibitory properties (Table 1). At first, the benzyl moiety of ChemBridge 7929959 and the phenyl moiety of 7933420 do not occupy the whole nucleotide-binding pocket. Instead, they occupy where the ribose moiety of ATP locates. Therefore, they do not work as a competitive inhibitor regarding ATP but as a mixed type. In the case of ChemBridge 7991890, the phenyl moiety is protruded outward due to the ethoxy group. As a result, the nucleotide-binding pocket is more spacious than the above two compounds. Therefore, the compound seems to function as an

uncompetitive inhibitor interacting with a catalytic product. Second, the substrate-binding pocket is not directly blocked by three compounds. The curved backbone of compounds occupies the interface of the substrate-binding pocket. Therefore, their inhibitory mode can be explained by a mixed type. It is worth to note that epigallocatechin gallate (EGCG) displays a competitive binding mode against both  $\beta$ -glucose-1-phosphate and ATP by occupying some parts of the substrate and nucleotide-binding regions<sup>24</sup>. Therefore, these *in silico* docking data provide a rational background to explain different binding modes of ChemBridge compounds and flavonoids.

The small  $K_i$  value of ChemBridge 7929959 indicates that it binds well in the substrate-binding site. Val32, Lys116, and Gly117 interact strongly with the compound compared with the other two compounds. In addition, Phe143 on the FEHDSST motif was predicted to have a critical role to recruit ATP through  $\pi$ - $\pi$  stacking interaction<sup>14</sup>. These properties seem to explain its 5.7- and 8.5-fold inhibitory activity compared with ChemBridge 7933420 and ChemBridge 7991890, respectively. The similar inhibitory mode of ChemBridge 7929959 and ChemBridge 7933420 may be originated from their benzyl and phenyl groups inserted into the hydrophobic pocket lined with Phe33, Tyr43, Leu44, Val56, and Leu85 (Figure 6). Actually, the morpholine moiety of MES is also located in the hydrophobic core<sup>14</sup>. However, the interaction of the oxadiazole ring of ChemBridge 7991890 with Lys69 and Tyr120 drew the 2-ethoxyphenyl group from the hydrophobic cavity. As a result, its position is a bit shifted to the surface compared with the other two ChemBridge compounds.

The catalytic activity of *BpHldC* was suppressed by ChemBridge 7929959 and its derivatives, ChemBridge 7933420 and 7991890.

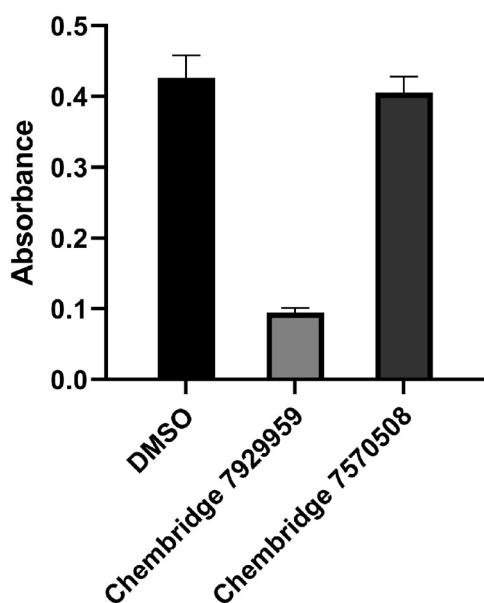


**Figure 7.** The comparison of reactivities of *BpHldC* with ChemBridge 7929959 and 7570508. The malachite assay was performed with 0.5 mM ATP and 1 mM  $\beta$ G1P. The observed absorbance could be considered as the reactivity of *BpHldC*. Compared to the control with DMSO, the reactivity of *BpHldC* with ChemBridge 7929959 fell meaningfully. However, the reactivity of *BpHldC* with ChemBridge 7570508 was almost not changed.

Therefore, the ChemBridge compounds possessed a molecular character strongly interacting with *BpHldC*. A detailed structural comparison was performed to guess which portion of the ChemBridge compounds was essential to inhibit the nucleotidyl-transferase activity of *BpHldC*. The three ChemBridge compounds shared the core structure, ethyl 5-[[[1,3,4-oxadiazol-2-yl]thio]acetyl]amino] 4-cyano-3-methyl -2-thiophene carboxylate, except the terminal aromatic groups (Figure 6(c–e)). Unlike the terminal benzyl ring of ChemBridge 7929959, ChemBridge 7933420 contains a chlorophenyl ring and an ethoxy phenyl ring for ChemBridge 7991890. In order to identify whether the terminal aromatic group is crucial to inhibit the catalytic activity of *BpHldC* or not, a commercially available compound with the closest core structure was purchased and assayed. It was ethyl 4-cyano-3-methyl-5-[[[4H-1,2,4-triazol-3-yl-thio]acetyl]amino]-2-thiophenecarboxylate (Chem Bridge 7570508) with exactly the same chemical formula with the core structure of the three ChemBridge compounds except for triazole at the terminal end. Therefore, the polarity of the terminal end is converted from negatively polar to neutral in ChemBridge 7570508. Nevertheless, the binding capability of the common core structure could be predictable because the polarity change is ignorable considering the size of the compounds. Intriguingly, the inhibitory activity of ChemBridge 7570508 was almost absent in the assay (Figure 7). The result clearly indicates that the aromatic rings (the benzyl or phenyl groups) in the three ChemBridge compounds are essential for binding together with endowing their different binding affinity to *BpHldC* (Figure 6).

In the previous study, we figured out that ChemBridge 7929959 inhibits *YpHddC*, the fourth enzyme of the GDP-6-deoxy- $\alpha$ -D-manno-heptose biosynthesis pathway<sup>16</sup>. However, their catalytic mechanisms are totally different. In the case of *YpHddC*, the catalytic site is designed to accept GTP in a lock-and-key fashion. In contrast, *BpHldC* adopts an induced-fit fashion triggering a huge conformational change of the C-terminal helix to perform its catalytic activity (Figure 8). As a result, their active site motifs and

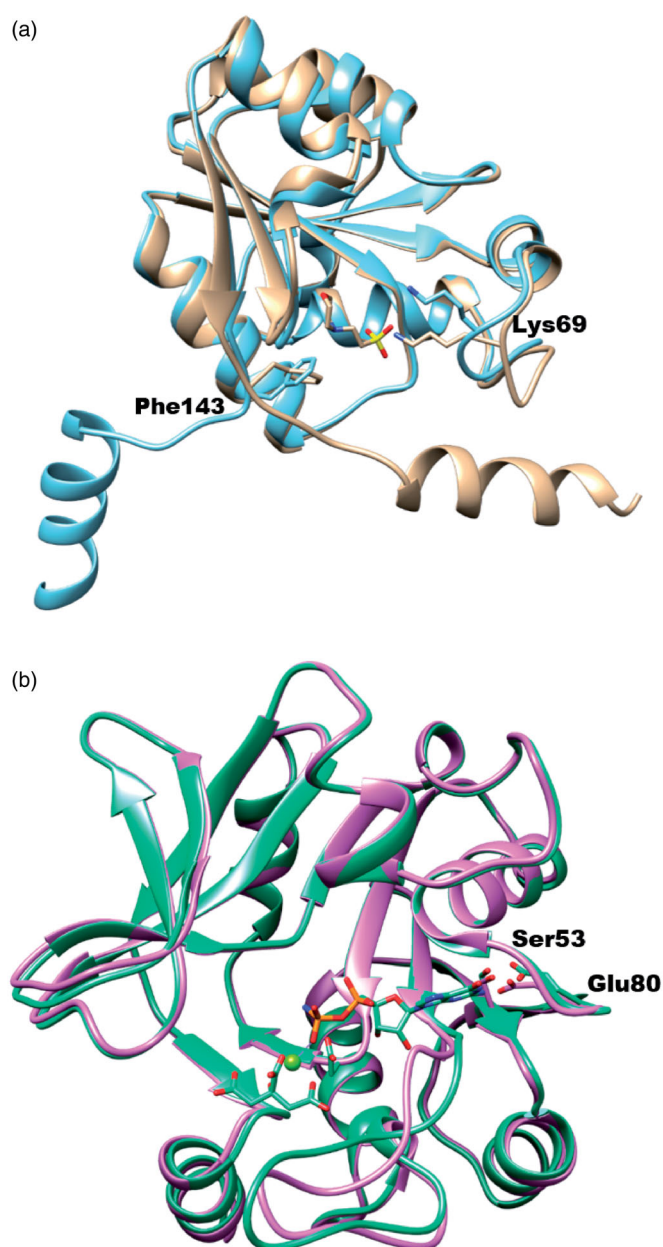


**Figure 8.** The superimposed ribbon diagrams of ligand-free and ligand-bound X-ray crystal structures of *BpHldC* and *YpHddC*. (a) The native (sky blue) and MES bound (tan) forms of *BpHldC* were drawn. (b) The native (orchid) and GMPPN (spring green) bound forms of *YpHddC* were drawn. A magnesium ion and a citrate molecules are also displayed. In both figures, catalytically important residues Lys69 and Phe143 were drawn with a stick model and labelled.

catalytic residues are different. Nevertheless, ChemBridge 7929959 functions as a dual inhibitor against *BpHldC* and *YpHddC*. The additional enzymatic studies have been performed to discern non-specific characteristics of the compound against various SNTs. However, ChemBridge 7929959 could not inhibit glucose-1-phosphate thymidyltransferase from *P. aeruginosa*, HddCs from *B. pseudomallei*, *C. jejuni*, *E. coli*, and *P. sp. 10(H)* and KdsBs from *B. pseudomallei*, *C. jejuni*, *C. psittaci*, *E. coli*, *K. aerogenes*, *N. meningitidis*, *P. aeruginosa*, *S. enterica*, and *V. cholerae*. Therefore, the compound shows selectivity against *BpHldC* and *YpHddC*. Since the dual inhibitory property is beneficial as antibiotics, a further study is going on to develop antibiotics targeting both HldC and HddC from the same pathogenic species. Currently, derivatives removing the ethyl-2-thiophenecarboxylate moiety from the core structure



are going on to define a minimal functional scaffold. In addition, derivatives adding functional groups to the benzyl moiety are being synthesised as a strategy to improve their binding affinity.

### Disclosure statement

No potential conflict of interest was reported by the author(s).

### Funding

This work was supported by the Basic Science Research Programs, 2018R1D1A1B07050781 to DHS and 2018R1D1A1B07050942 to MK, funded by the National Research Foundation of Korea Grant granted by the Ministry of Education, Science and Technology, Republic of Korea (MEST). S. Jo was supported by Brain Korea 21 (BK21) Project.

### References

1. Yabuuchi E, Kosako Y, Oyaizu H, et al. Proposal of *Burkholderia* gen. nov. and transfer of seven species of the genus *Pseudomonas* homology group II to the new genus, with the type species *Burkholderia cepacia* (Palleroni and Holmes 1981) comb. nov. *Microbiol Immunol* 1992;36: 1251–75.
2. Mahenthiralingam E, Urban TA, Goldberg JB. The multifarious, multireplicon *Burkholderia cepacia* complex. *Nat Rev Microbiol* 2005;3:144–56.
3. Compant S, Nowak J, Coenye T, et al. Diversity and occurrence of *Burkholderia* spp. in the natural environment. *FEMS Microbiol Rev* 2008;32:607–26.
4. Sawana A, Adeolu M, Gupta RS. Molecular signatures and phylogenomic analysis of the genus *Burkholderia*: proposal for division of this genus into the emended genus *Burkholderia* containing pathogenic organisms and a new genus *Paraburkholderia* gen. nov. harboring environmental species. *Front Genet* 2014;5:429.
5. Mahenthiralingam E, Baldwin A, Vandamme P. *Burkholderia cepacia* complex infection in patients with cystic fibrosis. *J Med Microbiol* 2002;51:533–8.
6. Biddick R, Spilker T, Martin A, LiPuma JJ. Evidence of transmission of *Burkholderia cepacia*, *Burkholderia multivorans* and *Burkholderia dolosa* among persons with cystic fibrosis. *FEMS Microbiol Lett* 2003;228:57–62.
7. Hauser AR, Jain M, Bar-Meir M, McColley SA. Clinical significance of microbial infection and adaptation in cystic fibrosis. *Clin Microbiol Rev* 2011;24:29–70.
8. Limmathurotsakul D, Peacock SJ. Melioidosis: a clinical overview. *Br Med Bull* 2011;99:125–39.
9. Brooke JS, Valvano MA. Biosynthesis of inner core lipopolysaccharide in enteric bacteria identification and characterization of a conserved phosphoheptose isomerase. *J Biol Chem* 1996;271:3608–14.
10. Brooke JS, Valvano MA. Molecular cloning of the *Haemophilus influenzae* gmhA (IpcA) gene encoding a phosphoheptose isomerase required for lipooligosaccharide biosynthesis. *J Bacteriol* 1996;178:3339–41.
11. Eidels L, Rick PD, Stimler NP, Osborn MJ. Transport of D-arabinose-5-phosphate and D-sedoheptulose-7-phosphate by the hexose phosphate transport system of *Salmonella typhimurium*. *J Bacteriol* 1974;119:138–43.
12. Raetz CR, Whitfield C. Lipopolysaccharide endotoxins. *Annu Rev Biochem* 2002;71:635–700.
13. Heinrichs DE, Valvano MA, Whitfield C. Biosynthesis and genetics of lipopolysaccharide core. In: Brade H, Morrison DC, Vogel S, Opal S, eds. *Endotoxin in health and disease*. New York: Marcel Dekker; 1999:305–30.
14. Park J, Kim H, Kim S, et al. Crystal structure of D-glycero-B-D-manno-heptose-1-phosphate adenylyltransferase from *Burkholderia pseudomallei*. *Proteins* 2018;86:124–31.
15. Valvano MA, Messner P, Kosma P. Novel pathways for biosynthesis of nucleotide-activated glycerol-manno-heptose precursors of bacterial glycoproteins and cell surface polysaccharides. *Microbiology (Reading)* 2002;148:1979–89.
16. Kim S, Jo S, Kim MS, Shin DH. A study of a potent inhibitor against a GDP-6-deoxy- $\alpha$ -D-manno-heptose biosynthesis pathway as antibiotic candidates. *Microb Drug Resist* 2020; 26:385–90.
17. Kim S, Jo S, Kim MS, Shin DH. A study of Rose Bengal against a 2-keto-3-deoxy-D-manno-octulosonate cytidylyltransferase as an antibiotic candidate. *J Enzyme Inhib Med Chem* 2020;35:1414–21.
18. Sha S, Zhou Y, Xin Y, Ma Y. Development of a colorimetric assay and kinetic analysis for *Mycobacterium tuberculosis* D-glucose-1-phosphate thymidyltransferase. *J Biomol Screen* 2012;17:252–7.
19. Zhang JH, Chung TD, Oldenburg KR. A simple statistical parameter for use in evaluation and validation of high throughput screening assays. *J Biomol Screen* 1999;4:67–73.
20. Sherman W, Day T, Jacobson MP, et al. Novel procedure for modeling ligand/receptor induced fit effects. *J Med Chem* 2006;49:534–53.
21. Jacobson MP, Pincus DL, Rapp CS, et al. A hierarchical approach to all-atom protein loop prediction. *Proteins* 2004; 55:351–67.
22. Friesner RA, Murphy RB, Repasky MP, et al. Extra precision glide: docking and scoring incorporating a model of hydrophobic enclosure for protein–ligand complexes. *J Med Chem* 2006;49:6177–96.
23. Strelow J, Dewe W, Iversen PW, et al. Mechanism of action assays for enzymes. In: Markossian S, et al., eds. *Assay guidance manual*. Bethesda (MD): Eli Lilly & Company and the National Center for Advancing Translational Sciences; 2004.
24. Kim S, Jo S, Kim MS, et al. Inhibition of D-glycero- $\beta$ -D-manno-heptose 1-phosphate adenylyltransferase from *Burkholderia pseudomallei* by epigallocatechin gallate and myricetin. *Biochem J* 2020;478:235–45.